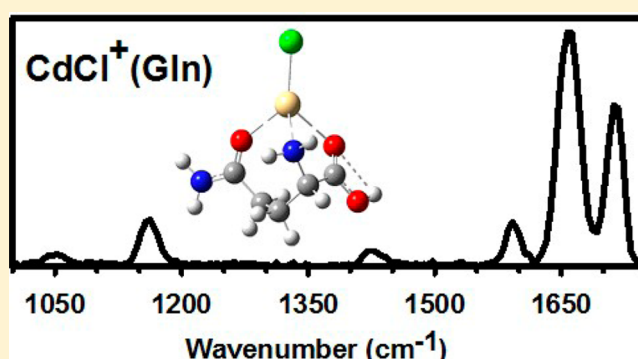


Experimental and Theoretical Investigations of Infrared Multiple Photon Dissociation Spectra of Glutamine Complexes with Zn^{2+} and Cd^{2+}

Georgia C. Boles,[†] Rebecca A. Coates,[†] Giel Berden,^{‡,§} Jos Oomens,^{‡,§} and P. B. Armentrout^{*,†}[†]Department of Chemistry, University of Utah, 315 South 1400 East Room 2020, Salt Lake City, Utah 84112, United States[‡]Institute for Molecules and Materials, FELIX Laboratory, Radboud University, Toernooiveld 7c, NL-6525 ED Nijmegen, The Netherlands[§]Van't Hoff Institute for Molecular Sciences, University of Amsterdam, Amsterdam, The Netherlands

Supporting Information

ABSTRACT: Complexes of glutamine (Gln) cationized with Zn^{2+} and Cd^{2+} were examined by infrared multiple photon dissociation (IRMPD) action spectroscopy using light generated from a free-electron laser. Electrospray ionization yielded complexes of deprotonated Gln with Zn^{2+} , $[\text{Zn}(\text{Gln}-\text{H})]^+$, and intact Gln with CdCl^+ , $\text{CdCl}^+(\text{Gln})$. For each complex, the spectra obtained were compared with those for low-energy conformers found using quantum chemical calculations to identify the structures present experimentally. Calculations were performed at the B3LYP/6-311+G(d,p) level for $[\text{Zn}(\text{Gln}-\text{H})]^+$ and at the B3LYP/def2-TZVP level with an SDD effective core potential on cadmium for $\text{CdCl}^+(\text{Gln})$. The main binding motif observed for the Cd^{2+} complex was a charge-solvated, tridentate $[\text{N},\text{CO},\text{CO}_{\text{sc}}]$ structure in which the metal binds to the backbone amino group and the carbonyl oxygens of the carboxylic acid and side-chain amide groups. The Zn^{2+} system similarly preferred a $[\text{N},\text{CO}^-,\text{CO}_{\text{sc}}]$ binding motif, where binding was observed at the carboxylate site along with the backbone amino and side-chain carbonyl groups. In both cases, the theoretically determined lowest-energy conformers explain the experimental $[\text{Zn}(\text{Gln}-\text{H})]^+$ and $\text{CdCl}^+(\text{Gln})$ spectra well.



INTRODUCTION

The physiological importance of the amino acid glutamine (Gln) has been well-documented, particularly through numerous studies involving the deamidation of Gln as well as asparagine (Asn) residues.^{1–7} Gln residues generally exhibit deamidation rates considerably slower than those of comparable peptide sequences containing Asn, although Gln deamidation has been shown to occur faster than Asn deamidation when Gln is located at the N-terminus.^{1,8,9} Specifically, solution-phase studies show that Gly–Xxx–Gln–Yyy–Gly pentapeptides (where Xxx and Yyy correspond to various amino acids) exhibit deamidation rates more than 10 times slower than those of Gly–Xxx–Asn–Yyy–Gly sequences.⁸ Therefore, monitoring Gln deamidation is particularly useful in studying degradation effects on long-lived proteins characterized by slow turnover rates as well as the detection and monitoring of bone degradation via MALDI MS.^{6,10} In addition to its deamidation properties, the use of Gln residues has also proved advantageous in other biologically important areas, such as tumor cell metabolism and therapeutics, as well as the advancement of enhanced selectivity of artificial ion channels.^{11–13}

In the present study, infrared multiple photon dissociation (IRMPD) action spectroscopy is utilized to characterize Gln complexes cationized with Zn^{2+} and Cd^{2+} . Zinc plays a significant role in binding to amino acid residues under biological conditions, particularly in various zinc-finger domains.^{14,15} Proteins containing zinc-finger domains participate in a wide range of biologically important functions, such as gene transcription and translation as well as mRNA trafficking.^{14,16,17} Here, it is important to note that the congener Cd^{2+} can replace Zn^{2+} within these domains, thus altering higher-order structure, deactivating the protein of its original function, and leading to toxicity.^{18,19} Although it is widely known that Zn^{2+} will bind preferentially to cysteine (Cys) and histidine (His) amino acid sites within proteins, as commonly observed in a Cys_2His_2 zinc-finger domain, it is not obvious why those particular amino acids are preferred. Previous IRMPD studies have evaluated the binding of metals, including Zn^{2+} and Cd^{2+} , with His, Cys, and CysOMe, thereby

Received: July 7, 2015

Revised: August 17, 2015

Published: August 17, 2015

elucidating important structural information regarding the metal dependence of these systems.^{20–23} In the current work, we continue our characterization of amino-acid binding with these two metal dications by extending these studies to Gln. From a fundamental point of view, such studies may help reveal why the functionalized side-chains of Cys and His (rather than of Gln) are favored binding sites.

In our previous work, electrospray ionization (ESI) of solutions of Cys (and CysOMe) or His with Zn^{2+} and Cd^{2+} yielded singly charged complexes of the deprotonated amino acid and metal, $[\text{M}(\text{AA}-\text{H})]^+$, along with singly charged complexes of the intact amino acid with CdCl^+ .^{21,23} Likewise, in the present study, ESI yields only $[\text{Zn}(\text{Gln}-\text{H})]^+$ and $\text{CdCl}^+(\text{Gln})$ complexes. To definitively determine the conformations of these species, we measured the experimental IRMPD action spectrum for the dissociation of each complex. Experimental spectra were then compared to the spectra calculated for a series of low-energy conformers, which allows clear identification of the conformation observed for each complex. Importantly, an extensive analysis of these complexes shows how the metal center affects the binding motif and other structural aspects of the metal–amino acid complexes, which allows for a more complete understanding of the metal-dependent binding to biologically relevant amino acids.

■ EXPERIMENTAL AND THEORETICAL METHODS

Mass Spectrometry and Photodissociation. Experiments were performed at the FELIX Facility of the Radboud University in The Netherlands using the free-electron laser for infrared experiments (FELIX) beamline.²⁴ A 4.7 T Fourier transform ion cyclotron resonance (FTICR) mass spectrometer, described elsewhere, was used to measure the IRMPD spectra.^{25–27} Ions were generated using an electrospray ionization source and then accumulated in a hexapole trap for about 5 s before being pulse-extracted through a quadrupole bender and injected into the ICR cell via a radiofrequency (rf) octopole ion guide. Electrostatic switching of the DC bias of the octopole was used to avoid collisional heating of the ions.²⁶ Once trapped in the ICR cell, the ion of interest (assumed to be roughly at room temperature) was mass-selected using a stored waveform inverse Fourier transform (SWIFT) excitation pulse. These ions were irradiated with FELIX for 2–3 s at a 10 Hz macropulse repetition rate (energy up to 45 mJ per pulse and bandwidth of 0.5% of the central frequency). The IRMPD spectra were generated by plotting the photofragmentation yield, $Y = \sum I_F / (\sum I_P + \sum I_F)$, where I_P and I_F are the integrated intensities of the parent and fragment ion mass peaks (where the sum includes all isotopes), respectively, as a function of the frequency of IR radiation. The yield is linearly corrected for frequency-dependent variation in the laser pulse energy. The application of a linear laser power correction is well-described in the literature³⁷ and is appropriate given that the power dependence is basically linear until saturation begins because of the incoherent rather than coherent nature of the multiple photon excitation process.

Metalated Gln complexes were prepared from solutions of 1.0 mM Gln and 1.0 mM $\text{Zn}(\text{NO}_3)_2$ or CdCl_2 in 60:40 MeOH/ H_2O using a Micromass Z-Spray ESI source. Flow rates of 6 $\mu\text{L}/\text{min}$ were used, and the electrospray needle was held at a voltage of 2.4 kV. In the case of the Zn^{2+} complex, the ESI source generated a $[\text{Zn}(\text{Gln}-\text{H})\text{ACN}]^+$ complex, in which the glutamine is deprotonated and ACN indicates acetonitrile. (The ACN was present adventitiously from previous experi-

ments.) In this case, a CO_2 laser was used to irradiate the sample for 0.3 s to remove the ACN ligand, leaving the $[\text{Zn}(\text{Gln}-\text{H})]^+$ complex. The resulting ions were mass-isolated and allowed to cool radiatively for 0.4 s.³⁰ Electrospray of the Cd^{2+} solution generated $\text{CdCl}^+(\text{Gln})$, which did not dissociate upon CO_2 laser irradiation.

Computational Details. To determine low-lying conformers of the cationized Gln complexes, we first optimized a series of 10–15 unique conformers of Gln at the B3LYP/6-311+G(d,p) level using the Gaussian 09 suite of programs.³¹ Initial optimizations of the metalated complexes were then done using the “loose” keyword to utilize a large step size of 0.01 au and an rms force constant of 0.0017 to facilitate convergence. Unique structures were then further optimized at the B3LYP/6-311+G(d,p) level of theory for Zn^{2+} complexes and at the B3LYP/def2-TZVP level, where def2TZVP is a size-consistent basis set for all atoms and includes triple- ζ + polarization functions with a small-core (28 electron) effective core potential (ECP) on Cd.^{32,33} The def2-TZVP basis set and corresponding ECP were obtained from the EMSL basis set exchange.³⁴ These combinations of level of theory, basis set, and ECP have previously proven to provide accurate structural information with complexes of similar size and composition.^{21,23,35} Geometry optimizations of metalated structures were also conducted including corrections for empirical dispersion at the B3LYP-GD3BJ level.³⁶

Vibrational frequencies were calculated at these levels of theory and were scaled by 0.975 for comparison to the IRMPD spectra. This scaling factor has been shown to account for known inaccuracies in the calculated frequencies and, therefore, gives good agreement with well-resolved peaks in other IRMPD spectra. The calculated frequencies were broadened using a 30 cm^{-1} full-width at half-maximum Gaussian line shape when used for comparison to the experimentally determined spectra. This broadening accounts for the finite laser bandwidth, unresolved rotational structure of the ions (which are near room temperature), anharmonicity of the vibrational mode, and broadening as a result of the multiple-photon absorption process.²⁹

Relative energies were determined for these B3LYP geometries using single-point energies calculated at the B3LYP, B3P86, and MP2(full) levels using 6-311+G(2d,2p) (Zn complexes) and def2-TZVPP (Cd complexes) basis sets. Zero-point energy (ZPE) corrections were applied to single-point energies to provide 0 K relative enthalpies. Thermal corrections to obtain 298 K Gibbs free energies were calculated as outlined previously from 0 K relative enthalpies by using the rigid rotor–harmonic oscillator approximation with the calculated rotational constants and vibrational frequencies.³⁵ Vibrational frequencies were scaled by 0.989 when used for ZPE and thermal corrections. Relative B3LYP-GD3BJ single-point energies using these larger basis sets and the B3LYP-GD3BJ geometries were also computed and are designated separately for comparison.

■ RESULTS AND DISCUSSION

IRMPD Action Spectroscopy. IRMPD action spectra for the complexes of Zn^{2+} and Cd^{2+} with Gln are shown in Figure 1. In the high-frequency range, the laser energy drops quickly, which results in a yield close to (or even higher than) one after correcting for the laser power. A yield greater than unity is an indication that the band would have been saturated if the laser power were higher. For each complex, the spectral region was

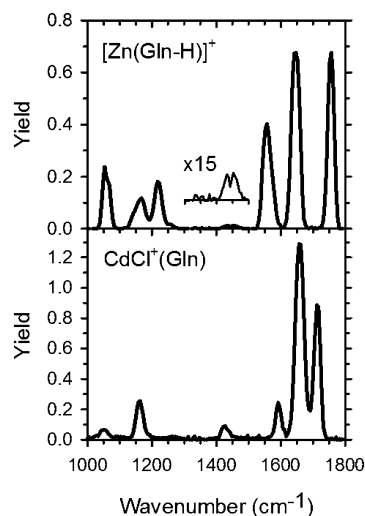
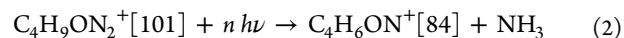
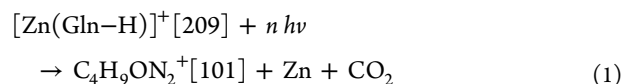


Figure 1. Infrared multiple photon dissociation action spectra of Zn^{2+} and Cd^{2+} complexes of Gln.

scanned from 5.5 to 10 μm (1000–1800 cm^{-1}), as there are no unique features in lower-frequency regions of the theoretically calculated spectra for all low-energy conformers.

Photodissociation of both $[\text{Zn}(\text{Gln}-\text{H})]^+$ and $\text{CdCl}^+(\text{Gln})$ complexes resulted in fragments corresponding to deamidation. Interestingly, the photodissociation process for which deamidation occurs is different, indicating that small changes in the local environment of the amino acid had a measurable effect on the deamidation process. IRMPD of the parent $[\text{Zn}(\text{Gln}-\text{H})]^+$ complex resulted in the fragmentation pattern corresponding to reactions 1 and 2, where the number in brackets indicates the mass to charge ratio (m/z) of the ion. Because ^{64}Zn is the most

abundant isotope (49.17% natural abundance), the complex of this isotope is designated here as the parent ion. Channels corresponding to ^{66}Zn and ^{68}Zn (27.73 and 18.45% natural abundance, respectively)³⁸ were also monitored and included in yield calculations shown in Figure 1.



The major product appeared at m/z 101 and resulted from the loss of ($\text{Zn} + \text{CO}_2$). As will be demonstrated below, the Gln ligand was deprotonated at the carboxylic acid site, such that CO_2 is a reasonable fragment, although why concomitant loss of the metal center occurs is not obvious. Deamidation in reaction 2 then occurred as a secondary loss from m/z 101. Interestingly, this shows that deamidation is preferred *after* the loss of the metal center, whereas in other systems (including Cd below), deamidation is observed with the metal center still participating in amino-acid binding.³⁵ Experimentally, the m/z 84 deamidation product generally had a significantly lower intensity (10–30%) compared to the m/z 101 fragment over most of the scanned frequency range. This observation is consistent with its identification as a secondary product, thus requiring a higher relative dissociation energy. However, the band near 1645 cm^{-1} showed enhanced intensity for the deamidation product, such that the intensities of the two fragment ions were nearly equal. This indicates that the m/z 101 fragment ion also absorbs strongly in this region of the spectrum, as verified computationally below.

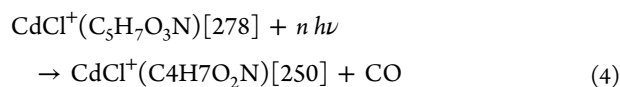
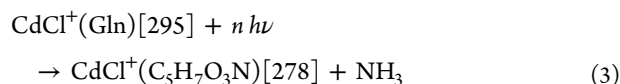
IRMPD of $\text{CdCl}^+(\text{Gln})$ resulted in two major fragments that appeared at m/z 278 and m/z 250, as shown in reactions 3 and 4. Here, masses are chosen to correspond to the most abundant

Table 1. Relative Enthalpies (0 K) and Free Energies (298 K) of $[\text{Zn}(\text{Gln}-\text{H})]^+$ Complexes^a

structure	B3LYP ^b	B3P86	MP2(full)
$[\text{N},\text{CO}^-, \text{CO}_{\text{sc}}^-]$ -gcgg	0.0 (0.0, 0.0)	0.0 (0.0)	0.0 (0.0)
$[\text{N},\text{CO}^-, \text{CO}_{\text{sc}}^-]$ -gggg	20.4 (20.5, 21.9)	21.3 (21.4)	24.2 (24.3)
$[\text{N},\text{CO}^-, \text{CO}_{\text{sc}}^-]$ -gtgt	21.0 (21.2, 22.2)	20.8 (21.0)	23.0 (23.3)
$[\text{N}^-, \text{CO}, \text{CO}_{\text{sc}}^-]$ -tgggg	45.0 (45.5, 49.4)	45.3 (45.8)	51.6 (52.1)
$[\text{N}^-, \text{CO}, \text{CO}_{\text{sc}}^-]$ -tgcgg	56.7 (57.5, 61.6)	56.8 (57.6)	60.0 (60.7)
$[\text{CO}_2^-, \text{CO}_{\text{sc}}^-]$ -gggg	61.1 (62.2)	64.7 (65.8)	70.9 (71.9)
$[\text{N}^-, \text{CO}, \text{CO}_{\text{sc}}^-]$ -cgcgg	66.5 (67.2)	67.2 (67.8)	73.1 (73.8)
$[\text{N}, \text{CO}^-, \text{N}_{\text{sc}}^-]$ -g-g-g-g+	72.4 (72.0)	72.2 (71.8)	57.9 (57.5)
$[\text{N}^-, \text{CO}, \text{CO}_{\text{sc}}^-]$ -cgggg	74.5 (75.4)	73.1 (74.0)	76.5 (77.5)
$[\text{N}, \text{C}_{\beta}^-, \text{CO}, \text{CO}_{\text{sc}}^-]$ -tgtgt	86.5 (88.3)	82.3 (84.1)	91.3 (93.1)
$[\text{N}, \text{C}_{\beta}^-, \text{CO}_{\text{sc}}^-]$ -tgggt	88.9 (90.6)	90.7 (92.5)	99.8 (101.6)
$[\text{N}^-, \text{OH}, \text{CO}_{\text{sc}}^-]$ -tg-cg-g-	89.9 (91.4)	95.0 (96.5)	94.2 (95.7)
$[\text{C}_{\alpha}^-, \text{CO}_{\text{sc}}^-]$ -ttggt	92.0 (95.2)	103.0 (106.1)	127.8 (130.9)
$[\text{N}, \text{CO}^-, \text{N}_{\text{sc}}^-]$ -g-g-g-g-	95.9 (95.8)	97.1 (97.0)	84.1 (84.0)
$[\text{N}^-, \text{OH}, \text{CO}_{\text{sc}}^-]$ -tg-cg-g-	98.2 (99.6)	102.2 (103.6)	98.6 (100.0)
$[\text{CO}, \text{C}_{\gamma}^-, \text{CO}_{\text{sc}}^-]$ -cggtg	99.6 (101.0)	95.3 (96.6)	112.7 (114.0)
$[\text{CO}^-, \text{CO}_{\text{sc}}^-]$ -gggg	102.1 (104.0)	109.3 (111.3)	112.5 (114.4)
$[\text{N}^-, \text{CO}_{\text{sc}}^-]$ -cgtgg	107.2 (108.3)	110.1 (111.2)	115.6 (116.7)
$[\text{N}, \text{CO}, \text{CO}_{\text{sc}}^-]$ -tgggg	110.6 (110.4)	111.3 (111.1)	106.9 (106.8)
$[\text{N}^-, \text{CO}, \text{N}_{\text{sc}}^-]$ -tgggg	112.3 (112.6)	112.7 (113.0)	103.4 (103.6)
$[\text{N}, \text{CO}^-]$ -gtgt	113.4 (114.3)	118.8 (119.6)	127.4 (128.3)
$[\text{CO}_2^-, \text{N}_{\text{sc}}^-]$ -gcgg	128.7 (129.9)	133.3 (134.5)	126.7 (127.8)
$[\text{N}^-, \text{CO}, \text{N}_{\text{sc}}^-]$ -cgggg	129.0 (129.5)	129.3 (129.8)	120.6 (121.1)

^aRelative single-point enthalpies and free energies (in parentheses) calculated at the level of theory indicated using a 6-311+G(2d,2p) basis set and B3LYP/6-311+G(d,p) geometries. ^bEmpirical-dispersion-corrected B3LYP-GD3BJ free energies (298 K) are given in bold for low-lying conformers.

isotopes of Cd and Cl, ^{114}Cd and ^{35}Cl , such that m/z 295 is designated as the parent ion. The complexes associated with m/z values corresponding to ^{113}Cd , ^{112}Cd , ^{111}Cd , ^{110}Cd , and ^{37}Cl were also monitored and included in yield calculations shown in Figure 1.



The fragment observed at m/z 278 is identified as the deamidation product, such that the conditions for deamidation are clearly distinct from those of the Zn^{2+} complex, as deamidation occurs with the metal center still participating in binding. Sequentially, the loss of CO is observed at higher energies (but no primary CO loss corresponding to m/z 267 was observed). These results are consistent with dissociation pathways previously found for complexes in which deamidation generally occurs as the primary loss, followed by the sequential loss of CO.^{5,39} Lower-intensity products include m/z 129, which is likely to correspond to the sequential loss of CdCl from m/z 278, and m/z 84, which is consistent with sequential loss of ($\text{NH}_3 + \text{CO}$) from m/z 129. Although these two product ions originate from all CdCl isotopes, their intensities were small, about 1 order of magnitude lower than that of m/z 250.

Theoretical Results: Relative Energies. As described above, a series of low-energy conformers of $[\text{Zn}(\text{Gln}-\text{H})]^+$ and $\text{CdCl}^+(\text{Gln})$ were found. Their resulting molecular parameters, including vibrational frequencies and single-point energies, were used to calculate their vibrational spectra and relative energies at 298 and 0 K. As given in Tables 1 and 2, enthalpies and free energies were calculated at the B3LYP, B3P86, and MP2(full) levels of theory and are given relative to the lowest-energy isomer at each level. Empirical-dispersion-corrected free energies were also calculated for low-lying conformers and are given in Tables 1 and 2 for comparison at the B3LYP level. Each of the complexes was named using nomenclature outlined previously.³⁵ In short, the complexes are designated by their metal-binding site in brackets, with the deprotonation site (if present) indicated by a negative sign. When deprotonation occurs at a carbon atom, carbons are designated with respect to their proximity to the carboxylic acid group, such that the adjacent carbon is defined as C_{α} . In cases where there is ambiguity regarding the two possible carbonyl- (and, in a few cases, nitrogen-) binding sites, a subscript sc is added to differentiate the side-chain group from the backbone group. The designation of the metal-binding site is then followed by the amino acid orientation, which is represented by the characterization of dihedral angles as cis (c, for angles between 0° and 45°), gauche (g, between 45° and 135°), or trans (t, between 135° and 180°). In a few cases, signs of the gauche angles (+ or -) are also needed to distinguish otherwise identical names. Dihedral angles were measured starting from the carboxylic acid hydrogen (unless this site is deprotonated) or the analogous proton on NH_2 in zwitterionic structures and going to the terminal side-chain nitrogen.

At all levels of theory, the predicted lowest-energy $[\text{Zn}(\text{Gln}-\text{H})]^+$ complex adopts a tridentate $[\text{N},\text{CO}^-, \text{CO}_{sc}]$ binding motif, where the metal binds to the backbone amino group, carbonyl

Table 2. Relative Enthalpies (0 K) and Free Energies (298 K) of $\text{CdCl}^+(\text{Gln})$ Complexes^a

structure	B3LYP ^b	B3P86	MP2(full)
$[\text{N},\text{CO},\text{CO}_{sc}]$ -tgccg	0.0 (0.0, 0.0)	0.0 (0.0)	0.0 (0.0)
$[\text{CO}_2^-]$ -ctggt	4.1 (4.0, 17.2)	3.5 (3.3)	16.4 (16.2)
$[\text{N},\text{CO},\text{CO}_{sc}]$ -tgggg	4.2 (4.0, 3.2)	3.8 (3.6)	2.7 (2.5)
$[\text{N},\text{CO},\text{CO}_{sc}]$ -tgtgt	16.0 (16.1, 16.1)	15.4 (15.4)	15.5 (15.5)
$[\text{N},\text{CO}]$ -tgtgt	16.9 (17.3, 24.0)	16.0 (16.4)	26.4 (26.7)
$[\text{N},\text{OH},\text{CO}_{sc}]$ -ttggg	29.3 (30.7, 25.9)	29.7 (31.1)	21.3 (22.7)
$[\text{N},\text{OH},\text{CO}_{sc}]$ -tgggg	29.9 (30.3, 29.2)	31.9 (32.3)	28.3 (28.7)
$[\text{N},\text{CO}_{sc}]$ -tgggt	30.0 (30.0)	31.8 (31.8)	34.7 (34.7)
$[\text{N},\text{CO}]$ -tctgt	30.6 (30.3)	30.3 (30.0)	42.3 (42.0)
$[\text{N},\text{CO}_{sc}]$ -ttggt	37.1 (38.1)	39.2 (40.1)	42.8 (43.8)
$[\text{N},\text{OH},\text{CO}_{sc}]$ -tgtgt	38.6 (39.2)	40.0 (40.5)	35.6 (36.1)
$[\text{N},\text{CO},\text{N}_{sc}]$ -tg-g-g-g+	42.0 (41.7)	39.0 (38.7)	28.2 (27.8)
$[\text{CO}^-, \text{CO}_{sc}]$ -cgggt	50.5 (51.2)	51.3 (51.9)	50.6 (51.3)
$[\text{N},\text{CO},\text{N}_{sc}]$ -tg-g-g-g-	52.1 (51.3)	49.4 (48.5)	36.3 (35.4)
$[\text{N},\text{OH}]$ -tgtgt	53.2 (53.1)	54.3 (54.2)	57.9 (57.8)
$[\text{N},\text{OH},\text{N}_{sc}]$ -tg-g-g-g+	82.6 (82.1)	82.0 (81.4)	65.1 (64.5)
$[\text{N},\text{OH},\text{N}_{sc}]$ -tg-g-g-g-	97.3 (96.8)	97.2 (96.7)	77.4 (76.9)
$[\text{N},\text{N}_{sc}]$ -tttgg	99.0 (99.0)	99.6 (99.6)	92.2 (92.1)
$[\text{CO},\text{N}_{sc}]$ -tgggt	119.2 (119.1)	123.3 (123.2)	123.6 (123.4)

^aRelative single-point enthalpies and free energies (in parentheses) calculated at the level of theory indicated using a def2-TZVPP basis set and corresponding ECP for Cd and B3LYP/def2-TZVP geometries.

^bEmpirical dispersion corrected B3LYP-GD3BJ free energies (298 K) are given in bold for low-lying conformers.

oxygen of the deprotonated carboxylic acid group, and carbonyl oxygen of the amide side-chain group. A total of three low-lying conformers of this type were located (Figure 2), although the gggg and gtgt variants lie 20–24 kJ/mol above the gcgg lowest-energy conformer, as shown in Table 1. The increased stability of the more compact gcgg conformer appears to be a subtle effect of the backbone orientation rather than of the combination of M–N and M–O bond distances, as those

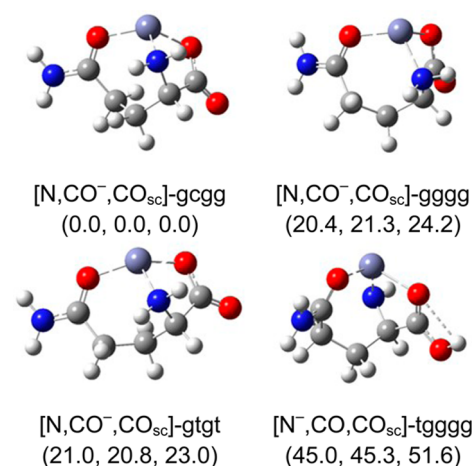


Figure 2. Structures of low-energy $[\text{Zn}(\text{Gln}-\text{H})]^+$ conformers calculated at the B3LYP/6-311+G(d,p) level of theory. Relative 0 K enthalpies (kJ/mol) are given at the B3LYP, B3P86, and MP2(full) levels, respectively. Shorter dashed lines indicate hydrogen bonds. Longer dashed lines indicate M–L bonds.

distances are very similar in all three $[\text{N},\text{CO}^-, \text{CO}_{\text{sc}}]$ conformers (within 0.03 and 0.01 Å, respectively). The two coordinates that appear to correlate with the relative energies are the M–N bond distances (2.06, 2.07, and 2.08 Å for gggg, gggg, and gtgt, respectively) and the NCCC dihedral angle (80° , 27° , and -18° , respectively), where deviations from $\pm 60^\circ$ impose unfavorable steric interactions, such that the gggg conformer clearly has a more staggered character than the gggg and gtgt variants. An estimate of the energy cost associated with such unfavorable dihedral angles can be obtained by considering a model butane system, where the energy difference between staggered (60°) and eclipsed methyl groups (0°) is roughly 15 kJ/mol.⁴⁰ This effect, in tandem with the shorter M–N distances, suggests that the energy difference observed between the three $[\text{N},\text{CO}^-, \text{CO}_{\text{sc}}]$ conformers is reasonable.

Tridentate structures where the amino group is deprotonated, $[\text{N}^-, \text{CO}, \text{CO}_{\text{sc}}]$, were also found, with the lowest energy variant (tgggg, Figure 2) lying 45–52 kJ/mol above the lowest energy conformer. Bidentate structures are considerably higher in energy than the tridentate conformers (92–128 kJ/mol higher than the lowest energy conformer). When B3LYP results are corrected for empirical dispersion factors, the corrected relative energies more closely agree with MP2(full) values (especially for the higher-energy conformers). Better correlation between B3LYP-GD3BJ values and MP2(full) theory, which accounts for electron correlation effects more accurately, has also been shown with other small peptide systems.⁴¹

The lowest-energy conformers of $\text{CdCl}^+(\text{Gln})$ also favor a tridentate binding motif, as previously found for other amino acids (see Table 2 and Figure 3).^{35,42} Specifically, there are three low-lying structures of $\text{CdCl}^+(\text{Gln})$ that exhibit a $[\text{N}, \text{CO}, \text{CO}_{\text{sc}}]$ conformation in which the metal binds to the backbone amino group, carbonyl oxygen of the carboxylic acid group, and carbonyl oxygen of the of the amide group. Low-lying bidentate structures, namely $[\text{N}, \text{CO}^-]-\text{tgtgt}$ and $[\text{N}, \text{CO}_{\text{sc}}]-\text{tgggt}$, were also located; however, the lowest-energy bidentate structure is a zwitterionic $[\text{CO}_2^-]-\text{ctggt}$ conformer, where the hydrogen of the carboxylic acid transfers to the backbone amino group, which also hydrogen-bonds to the carbonyl oxygen of the amide. This conformer is only 3–4 kJ/mol higher in energy than the lowest-energy conformer at the B3LYP and B3P86 levels but 16–17 kJ/mol higher for MP2(full) and B3LYP-GD3BJ. This zwitterionic binding motif is also exhibited by low-energy conformers of Gln complexes cationized with Li^+ , Na^+ , K^+ , and Cs^+ .⁴² Analogous $[\text{N}, \text{OH}, \text{CO}_{\text{sc}}]$ structures are also found but lie 20–30 kJ/mol higher in energy than the equivalent $[\text{N}, \text{CO}, \text{CO}_{\text{sc}}]$ conformers. As shown in Table 2, accounting for empirical dispersion has much larger effects on the relative energies of $\text{CdCl}^+(\text{Gln})$ complexes than those found for $[\text{Zn}(\text{Gln}-\text{H})]^+$. It is clear that dispersion corrections bring the B3LYP results more in line with the MP2(full) results.

Theoretical Results: $[\text{Zn}(\text{Gln}-\text{H})]^+$ Structures. A full description of the key geometric parameters of each identified binding motif is given in Tables 3 and 4. This structural analysis is particularly advantageous for analyzing the relative binding strength and conformational changes observed for each complex. All $[\text{Zn}(\text{Gln}-\text{H})]^+$ complexes exhibit shorter M–O and M–O_{sc} distances than do the $\text{CdCl}^+(\text{Gln})$ complexes characterized by a similar binding motif. This reflects the smaller ionic radius of Zn^{2+} (0.60 Å) as compared to that of Cd^{2+} (0.78 Å),⁴³ as well as tighter binding in the $[\text{Zn}(\text{Gln}-\text{H})]^+$ complexes as a result of stronger electrostatic interactions

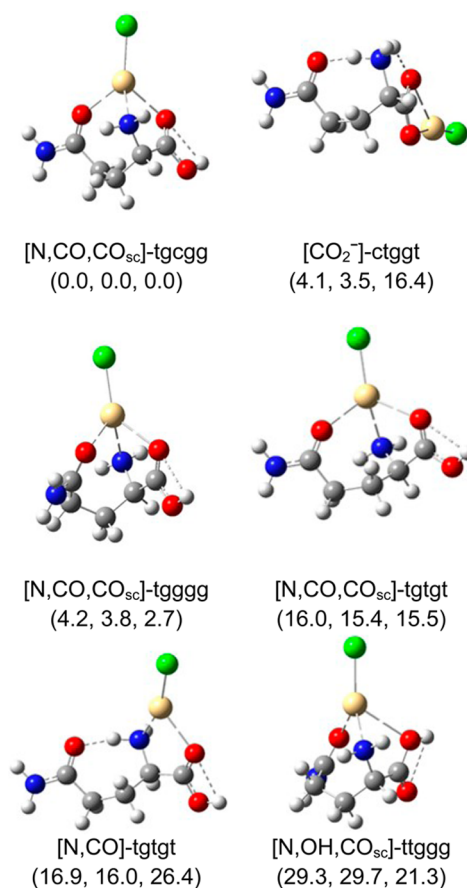


Figure 3. Structures of low-energy $\text{CdCl}^+(\text{Gln})$ conformers calculated at the B3LYP/def2-TZVP level of theory. Relative single-point enthalpies (0 K) are given at the B3LYP, B3P86, and MP2(full) levels, respectively. Shorter dashed lines indicate hydrogen bonds. Longer dashed lines indicate M–L bonds.

between the metal center and carboxylate anion as compared with the carboxylic acid group in the Cd^{2+} complexes.

Of the $[\text{Zn}(\text{Gln}-\text{H})]^+$ structures characterized by a tridentate $[\text{N}, \text{CO}^-, \text{CO}_{\text{sc}}]$ binding motif, the M–O and M–N distances are nearly identical, and there is no direct correlation of $\angle \text{NMO}$, $\angle \text{NMO}_{\text{sc}}$, and $\angle \text{OMO}_{\text{sc}}$ angles playing a significant role in the relative energies of these conformers. As discussed above, the difference in energetics can be correlated with the backbone orientation, specifically the NCCC dihedral angle (80° , 27° , and -18° , respectively). As shown by the $[\text{N}^-, \text{CO}, \text{CO}_{\text{sc}}]$ conformers, deprotonation at the backbone nitrogen significantly decreases the M–N distances and increases the M–O distances, while the M–O_{sc} distance remains similar to those observed in the $[\text{N}, \text{CO}^-, \text{CO}_{\text{sc}}]$ conformers. Interestingly, whereas the $[\text{N}, \text{CO}^-, \text{CO}_{\text{sc}}]$ structures prefer to be more compact, the $[\text{N}^-, \text{CO}, \text{CO}_{\text{sc}}]$ conformers favor a more open chain. A total of two $[\text{N}, \text{CO}^-, \text{N}_{\text{sc}}]$ conformations were found, and they have M–O and M–N distances similar to those of the $[\text{N}, \text{CO}^-, \text{CO}_{\text{sc}}]$ conformers but longer M–N_{sc} distances compared to those of M–O_{sc}. Likewise two $[\text{N}^-, \text{CO}, \text{N}_{\text{sc}}]$ conformers form a similar comparison with $[\text{N}^-, \text{CO}, \text{CO}_{\text{sc}}]$ conformers. The CO_{sc} binding site is clearly energetically favored compared to that of N_{sc}, as the $[\text{N}, \text{CO}^-, \text{N}_{\text{sc}}]$ conformers are 58–97 kJ/mol higher in energy than the lowest-energy $[\text{N}, \text{CO}^-, \text{CO}_{\text{sc}}]$ conformer, and $[\text{N}^-, \text{CO}, \text{N}_{\text{sc}}]$ are 52–84 kJ/mol above the lowest energy

Table 3. Bond Distances (Å) and Bond Angles (deg) for $[\text{Zn}(\text{Gln}-\text{H})]^+$ Structures^a

structure	$r(\text{M}-\text{X})$	$r(\text{M}-\text{O})$	$r(\text{M}-\text{Y}_{\text{sc}})$	$\angle\text{XMO}$	$\angle\text{XMY}_{\text{sc}}$	$\angle\text{OMY}_{\text{sc}}$
$[\text{N},\text{CO}^-, \text{CO}_{\text{sc}}]-\text{gcgg}$	2.06	1.88	1.93	88.5	104.7	125.6
$[\text{N},\text{CO}^-, \text{CO}_{\text{sc}}]-\text{gggg}$	2.07	1.89	1.93	87.8	111.7	116.6
$[\text{N},\text{CO}^-, \text{CO}_{\text{sc}}]-\text{gtgt}$	2.08	1.88	1.93	87.3	103.9	135.7
$[\text{N}^-, \text{CO}, \text{CO}_{\text{sc}}]-\text{tgggg}$	1.90	2.15	1.95	88.3	116.9	98.0
$[\text{N}^-, \text{CO}, \text{CO}_{\text{sc}}]-\text{tgcgg}$	1.87	2.14	1.95	84.1	122.2	105.4
$[\text{CO}_2^-, \text{CO}_{\text{sc}}]-\text{gggg}$	2.00 ^b	2.02	1.92	66.3 ^b	107.3 ^b	105.8
$[\text{N}^-, \text{CO}, \text{CO}_{\text{sc}}]-\text{cgcgg}$	1.90	2.15	1.94	87.9	114.5	106.5
$[\text{N}, \text{CO}^-, \text{N}_{\text{sc}}]-\text{g}_-\text{g}_+\text{g}_+$	2.06	1.87	2.05 ^c	89.1	109.5 ^c	120.3 ^c
$[\text{N}^-, \text{CO}, \text{CO}_{\text{sc}}]-\text{cgggg}$	1.88	2.10	1.95	85.1	123.9	96.1
$[\text{N}, \text{C}_{\beta}^-, \text{CO}, \text{CO}_{\text{sc}}]-\text{tgtgt}$	2.31/2.03 ^d	2.38	2.07	72.0/82.6 ^d	95.9/89.9 ^d	167.5
$[\text{N}, \text{C}_{\beta}^-, \text{CO}_{\text{sc}}]-\text{tgggt}$	2.15/2.03 ^d		2.05		111.8/88.6 ^d	
$[\text{N}^-, \text{OH}, \text{CO}_{\text{sc}}]-\text{tg}_-\text{cg}_+\text{g}_-$	1.86	2.39 ^e	1.91	81.3 ^e	125.5	100.3 ^e
$[\text{C}_{\alpha}^-, \text{CO}_{\text{sc}}]-\text{ttggt}$	2.17 ^d		2.01		108.4 ^d	
$[\text{N}, \text{CO}^-, \text{N}_{\text{sc}}]-\text{g}_+\text{g}_-\text{g}_-$	2.06	1.87	2.04 ^c	88.4	114.3 ^c	117.0 ^c
$[\text{N}^-, \text{OH}, \text{CO}_{\text{sc}}]-\text{tg}_+\text{cg}_-\text{g}_+$	1.86	2.26 ^e	1.92	79.4 ^e	130.7	99.4 ^e
$[\text{CO}, \text{C}_{\gamma}^-, \text{CO}_{\text{sc}}]-\text{cgggtg}$	2.02 ^d	1.97	2.12	109.6 ^d	69.6 ^d	125.5
$[\text{CO}^-, \text{CO}_{\text{sc}}]-\text{gggg}$		1.80	1.87			145.5
$[\text{N}^-, \text{CO}_{\text{sc}}]-\text{cgtgg}$	1.83		1.89		139.0	
$[\text{N}, \text{CO}, \text{CO}_{\text{sc}}^-]-\text{tgggg}$	2.10	2.05	1.83	81.0	109.8	129.8
$[\text{N}^-, \text{CO}, \text{N}_{\text{sc}}]-\text{tgggg}$	1.89	2.12	2.07 ^c	88.7	117.0 ^c	99.6 ^c
$[\text{N}, \text{CO}^-]-\text{tgtgt}$	1.97	1.85		97.2		
$[\text{CO}_2^-, \text{N}_{\text{sc}}]-\text{gcgg}$	2.01 ^b	2.01	2.06 ^c	66.4 ^b	102.1 ^{b,c}	106.5 ^c
$[\text{N}^-, \text{CO}, \text{N}_{\text{sc}}]-\text{cgggg}$	1.88	2.11	2.06 ^c	88.1	113.9 ^c	102.3 ^c

^aValues calculated at the B3LYP/6-311+G(d,p) level of theory. Except as noted, O indicates carbonyl oxygen of backbone, Y_{sc} indicates carbonyl oxygen of the side-chain, and X indicates amino nitrogen. ^bX: second oxygen in carboxylate group. ^c Y_{sc} : side chain nitrogen. ^dX: backbone carbon. ^eO: hydroxyl group oxygen.

Table 4. Bond Distances (Å) and Bond Angles (deg) for $\text{CdCl}^+(\text{Gln})$ Structures^a

structure	$r(\text{M}-\text{X})$	$r(\text{M}-\text{O})$	$r(\text{M}-\text{Y}_{\text{sc}})$	$\angle\text{XMO}$	$\angle\text{XMY}_{\text{sc}}$	$\angle\text{OMY}_{\text{sc}}$
$[\text{N}, \text{CO}, \text{CO}_{\text{sc}}]-\text{tgcgg}$	2.35	2.41	2.28	70.9	81.3	95.3
$[\text{CO}_2^-]-\text{ctggt}$	2.55 ^b	2.15		55.5 ^b		
$[\text{N}, \text{CO}, \text{CO}_{\text{sc}}]-\text{tgggg}$	2.41	2.38	2.27	69.4	89.3	79.0
$[\text{N}, \text{CO}, \text{CO}_{\text{sc}}]-\text{tgtgt}$	2.34	2.44	2.32	69.8	80.2	105.2
$[\text{N}, \text{CO}]-\text{tgtgt}$	2.23	2.38		73.5		
$[\text{N}, \text{OH}, \text{CO}_{\text{sc}}]-\text{ttggg}$	2.34	2.63 ^c	2.23	63.1 ^c	90.6	77.6 ^c
$[\text{N}, \text{OH}, \text{CO}_{\text{sc}}]-\text{tgggg}$	2.32	2.58 ^c	2.23	66.2 ^c	84.9	99.0 ^c
$[\text{N}, \text{CO}_{\text{sc}}]-\text{tgggt}$	2.26		2.25		91.1	
$[\text{N}, \text{CO}]-\text{tctgt}$	2.21	2.42		71.5		
$[\text{N}, \text{CO}_{\text{sc}}]-\text{ttggt}$	2.27		2.24		91.8	
$[\text{N}, \text{OH}, \text{CO}_{\text{sc}}]-\text{tgtgt}$	2.28	2.77 ^c	2.29	63.2 ^c	82.3	114.1 ^c
$[\text{N}, \text{CO}, \text{N}_{\text{sc}}]-\text{tg}_-\text{g}_+\text{g}_+$	2.33	2.35	2.65 ^d	72.3	89.6 ^d	93.8 ^d
$[\text{CO}^-, \text{CO}_{\text{sc}}]-\text{cgggt}$		2.12	2.43			77.0
$[\text{N}, \text{CO}, \text{N}_{\text{sc}}]-\text{tg}_-\text{g}_+\text{g}_-$	2.38	2.30	2.57 ^d	71.3	95.8 ^d	87.8 ^d
$[\text{N}, \text{OH}]-\text{tgtgt}$	2.17	2.54 ^c		70.2 ^c		
$[\text{N}, \text{OH}, \text{N}_{\text{sc}}]-\text{tg}_-\text{g}_+\text{g}_+$	2.27	2.50 ^c	2.57 ^d	68.9 ^c	92.4 ^d	96.0 ^{c,d}
$[\text{N}, \text{OH}, \text{N}_{\text{sc}}]-\text{tg}_+\text{g}_-\text{g}_-$	2.31	2.47 ^c	2.47 ^d	68.0 ^c	97.6 ^d	90.0 ^{c,d}
$[\text{N}, \text{N}_{\text{sc}}]-\text{tttgg}$	2.23		2.55 ^d		93.4 ^d	
$[\text{CO}, \text{N}_{\text{sc}}]-\text{tgggt}$		2.18	2.42 ^d			90.3 ^d

^aValues calculated at the B3LYP/def2-TZVP level of theory. Except as noted, O indicates carbonyl oxygen of backbone, Y_{sc} indicates carbonyl oxygen of the side-chain, and X indicates amino nitrogen. ^bX: second oxygen in carboxylate group. ^cO: hydroxyl oxygen. ^d Y_{sc} : side chain nitrogen.

$[\text{N}^-, \text{CO}, \text{CO}_{\text{sc}}]$. Again, the orientation of dihedral angles seem to be important, as the $[\text{N}^-, \text{CO}, \text{N}_{\text{sc}}]-\text{g}_-\text{g}_+\text{g}_+$ conformer is 23–26 kJ/mol lower in energy than the $\text{g}_+\text{g}_-\text{g}_-$ conformer. Deprotonation at the amino group also allows $[\text{N}^-, \text{OH}, \text{CO}_{\text{sc}}]$ conformations, which have much longer M–OH bonds than in the $[\text{N}^-, \text{CO}, \text{CO}_{\text{sc}}]$ conformers, something that is also reflected in their high relative energies of 90–102 kJ/mol. A total of two conformers, $[\text{CO}_2^-, \text{CO}_{\text{sc}}]$ and $[\text{CO}_2^-, \text{N}_{\text{sc}}]$, were found with

binding at both oxygens of the carboxylate group and nearly identical M–O bond distances. Again, the CO_{sc} conformer is much lower in energy than the N_{sc} conformer. Finally, one $[\text{N}, \text{CO}, \text{CO}_{\text{sc}}^-]$ conformer has a significantly shorter M–O_{sc} distance than any other conformer (1.83 Å) as a result of deprotonation at this site.

A total of two tridentate structures, $[\text{N}, \text{C}_{\beta}^-, \text{CO}_{\text{sc}}]-\text{tgggt}$ and $[\text{CO}, \text{C}_{\gamma}^-, \text{CO}_{\text{sc}}]-\text{cgggtg}$, were found where the metal binds at a

deprotonated carbon. Understandably, these conformers exhibit relatively short M–C distances (~ 2.0 Å), with the other metal–ligand bond distances being comparable to many of the other tridentate conformers. One distinction in these two cases is that the $\angle \text{CMO}_{\text{sc}}$ angle in $[\text{N}, \text{C}_{\beta}^-, \text{CO}_{\text{sc}}^-] \text{-tggt}$ is significantly larger than that in $[\text{CO}, \text{C}_{\gamma}^-, \text{CO}_{\text{sc}}^-] \text{-cggtg}$, which exhibits the smallest angle of any conformation. Deprotonation at a carbon also leads to the only tetradentate $[\text{N}, \text{C}_{\beta}^-, \text{CO}, \text{CO}_{\text{sc}}^-]$ species, lying 82–91 kJ/mol above the lowest-energy conformer. Of all of the located conformations, this conformer exhibits the longest M–O, M–N, and M–O_{sc} distances and, again, a short M–C bond distance. The $\angle \text{CMO}_{\text{sc}}$ angles found for both species deprotonating at the C_β site were found to be fairly similar.

Several high-energy bidentate conformations were found and exhibit short M–O and M–O_{sc} distances (1.80–2.01 Å, respectively). These complexes have the shortest bond distances among all conformers, with $[\text{CO}^-, \text{CO}_{\text{sc}}^-] \text{-gggg}$ having $r(\text{M–O}) = 1.80$ Å and $r(\text{M–O}_{\text{sc}}) = 1.87$ Å, and $[\text{N}^-, \text{CO}_{\text{sc}}^-] \text{-cgtgg}$ having $r(\text{M–N}) = 1.83$ Å. This suggests tight binding in these bidentate conformations; however, because these structures are relatively high in energy, the presence of the additional binding site in the tridentate conformations is clearly important. The lowest-energy bidentate structure (still 92–128 kJ/mol above the lowest-energy conformer) is the $[\text{C}_{\alpha}^-, \text{CO}_{\text{sc}}^-]$ conformer, the only bidentate conformer with deprotonation occurring at a carbon. This complex exhibits relatively long M–X (where X = C_α) and M–O_{sc} distances (2.17 and 2.01 Å, respectively).

Theoretical Results: CdCl(Gln)⁺ Structures. For the CdCl⁺(Gln) complex, three $[\text{N}, \text{CO}, \text{CO}_{\text{sc}}^-]$ conformations (including the lowest-energy tgctg conformer) were found. Similarly to the $[\text{N}, \text{CO}^-, \text{CO}_{\text{sc}}^-]$ conformers of the $[\text{Zn}(\text{Gln–H})]^+$ system, the energy distribution of these conformers appear to be a subtle effect of the side-chain orientation, specifically the NCCC dihedral angle (79°, –39°, and 32° for tgctg, tgggg, and tgtgt, respectively). Again, deviations from $\pm 60^\circ$ result in unfavorable energetics, such that angles in the lowest-energy conformer deviate the least. Analogous $[\text{N}, \text{OH}, \text{CO}_{\text{sc}}^-]$ conformations were found to lie 20–30 kJ/mol above the $[\text{N}, \text{CO}, \text{CO}_{\text{sc}}^-]$ conformer, having the comparable backbone configuration. These three conformers exhibit M–N and M–O_{sc} distances comparable to (although generally slightly less than) those of the $[\text{N}, \text{CO}, \text{CO}_{\text{sc}}^-]$ conformers, but the M–OH distances (2.58–2.77 Å) are much longer than the analogous M–OC distances (2.38–2.44 Å) in the $[\text{N}, \text{CO}, \text{CO}_{\text{sc}}^-]$ conformers. If the side-chain binding site switches from CO_{sc} to N_{sc}, two $[\text{N}, \text{CO}, \text{N}_{\text{sc}}^-]$ conformers are found and lie 28–52 kJ/mol above the lowest-energy conformer. Likewise, two comparable $[\text{N}, \text{OH}, \text{N}_{\text{sc}}^-]$ conformers, lying another 37–48 kJ/mol higher, were also located. Again, slight conformational changes in the $[\text{N}, \text{CO}, \text{N}_{\text{sc}}^-]$ and $[\text{N}, \text{OH}, \text{N}_{\text{sc}}^-]$ conformers have only a small effect on the M–N and M–O distances (where the $[\text{N}, \text{OH}, \text{N}_{\text{sc}}^-]$ conformers have slightly shorter M–N distances), but the M–N_{sc} distance is about 0.09 Å shorter in the $[\text{N}, \text{OH}, \text{N}_{\text{sc}}^-]$ conformers compared to those in the analogous lower-energy $[\text{N}, \text{CO}, \text{N}_{\text{sc}}^-]$ counterparts.

Many bidentate structures were located, with the most stable being the zwitterionic $[\text{CO}_2^-]$ conformation. Here, the metal does not bind equally to both oxygens, but rather, the M–O distances differ by 0.4 Å, with the longer distance corresponding to the oxygen, making a hydrogen bond to the NH₃⁺ group. Low-lying bidentate conformations $[\text{N}, \text{CO}]$ and

$[\text{N}, \text{CO}_{\text{sc}}^-]$ exhibit M–O and M–O_{sc} distances slightly less and M–N distances about 0.1 Å less than the lowest-energy tridentate conformer, indicating that there is decreased steric strain in these bidentate conformations. An additional zwitterionic $[\text{CO}^-, \text{CO}_{\text{sc}}^-]$ conformation was found 50–51 kJ/mol above the lowest-energy conformer. Compared with the $[\text{CO}_2^-] \text{-cggtg}$ conformation, both M–O distances are shorter in the $[\text{CO}^-, \text{CO}_{\text{sc}}^-]$ complex, which might indicate tighter binding; however, this complex has obvious steric effects regarding the dihedral angles that account for the increase in energy. Additional high-energy forms include $[\text{N}, \text{OH}]$, $[\text{N}, \text{N}_{\text{sc}}^-]$, and $[\text{CO}, \text{N}_{\text{sc}}^-]$, which all have shorter bonds than analogous tridentate conformers.

Comparison of Experimental and Theoretical IR Spectra: $[\text{Zn}(\text{Gln–H})]^+$. In comparing the experimental and theoretical IR spectra, it should be remembered that the experimental IRMPD intensities are not always reproduced by the calculated one-photon linear absorption spectrum; however, infrared spectra obtained using IRMPD methods are generally comparable to those recorded using linear absorption techniques, in part because the spectra result from incoherent, rather than coherent, multiple photon excitation. Previous modeling studies have demonstrated the near-linear absorption character of IRMPD studies.^{28,29}

As shown in Figure 4, the most intense spectral features in the computed spectra of the lowest-energy $[\text{N}, \text{CO}^-, \text{CO}_{\text{sc}}^-]$

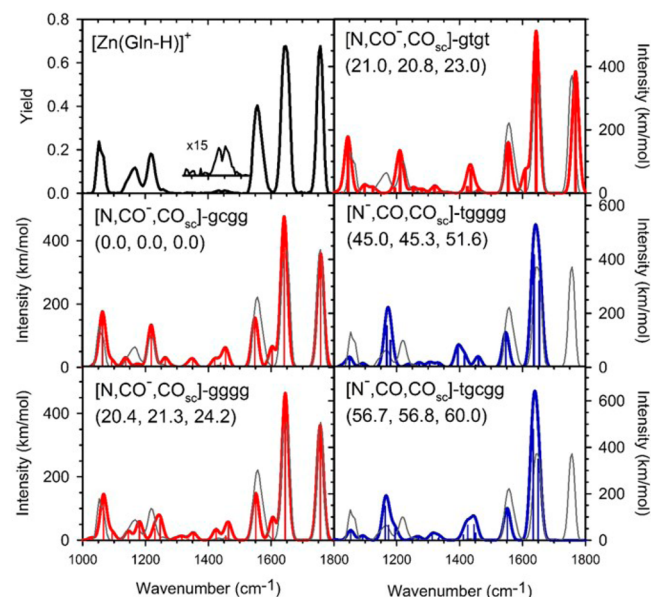


Figure 4. Comparison of the $[\text{Zn}(\text{Gln–H})]^+$ experimental IRMPD action spectrum with IR spectra calculated at the B3LYP/6-311+G(d,p) level of theory for low-lying conformers. Relative 0 K enthalpies (kJ/mol) are given at the B3LYP, B3P86, and MP2(full) levels, respectively.

conformers correlate well with those observed in the experimental $[\text{Zn}(\text{Gln–H})]^+$ spectrum. Specifically, the bands at 1557 (amide NH₂ bend and CO stretch), 1647 (amide NH₂ bend), and 1757 cm^{–1} (stretch of uncoordinated CO in carboxylate) in the $[\text{Zn}(\text{Gln–H})]^+$ spectrum are consistent with those exhibited in the $[\text{N}, \text{CO}^-, \text{CO}_{\text{sc}}^-] \text{-gctgg}$ and $[\text{N}, \text{CO}^-, \text{CO}_{\text{sc}}^-] \text{-gggg}$ conformers, both in band frequency and relative intensity, whereas in the $[\text{N}, \text{CO}^-, \text{CO}_{\text{sc}}^-] \text{-gtgt}$ spectrum, the 1757 cm^{–1} band is predicted to lie about 10 cm^{–1} higher in

wavenumber. There is also reasonable agreement among these spectra for the band at 1053 cm^{-1} (amino NH_2 wag) in the $[\text{Zn}(\text{Gln}-\text{H})]^+$ spectrum, with deviations being a red shift of 19 cm^{-1} in the $[\text{N},\text{CO}^-, \text{CO}_{\text{sc}}]-\text{gtgt}$ spectrum. The main distinction among these spectra arises from the band at 1218 cm^{-1} (CCH bend, CO stretch, and additional contributions from NH_2 and CH_2 rock) in the experimental spectrum, as only the $[\text{N},\text{CO}^-, \text{CO}_{\text{sc}}]-\text{gcgg}$ conformer exhibits a peak in good agreement with this frequency (and also predicts a weak band consistent with the shoulder observed at a higher frequency). A small red shift ($\sim 8\text{ cm}^{-1}$) of the same band is seen in the gtgt spectrum, where the motions are comparable with some enhancement of the NH_2 rock. For the gggg conformer, the band shifts to the blue and weakens with a band at 1230 cm^{-1} (CO stretch and NH_2 and CH_2 rock) and 1246 cm^{-1} (CCH bend and CH_2 rock). The gcgg and gggg conformers also reproduce the weak bands observed at 1434 and 1454 cm^{-1} (primarily backbone CH_2 wagging), whereas gtgt predicts a single moderately intense band in this frequency range.

The main feature in the experimental spectrum not well reproduced by the $[\text{N},\text{CO}^-, \text{CO}_{\text{sc}}]-\text{gcgg}$ conformer appears at 1160 cm^{-1} , although there are weak bands in this spectrum at this frequency. The $[\text{N},\text{CO}^-, \text{CO}_{\text{sc}}]-\text{gggg}$ spectrum reproduces this band better, with a peak at 1181 cm^{-1} and a shoulder at 1146 cm^{-1} . We also note that there is a band predicted in all $[\text{N},\text{CO}^-, \text{CO}_{\text{sc}}]$ spectra at 1604 cm^{-1} that corresponds to the bend of the backbone amino NH_2 group; however, this band is not reproduced in the experimental spectrum at that frequency. This phenomenon has been observed in many other amino acid systems, where it was concluded that strong anharmonic effects in the NH_2 bend result in a red shift of about 25 cm^{-1} .^{20,23,44–48} Here, such a shift would lead this band to overlap the band centered at 1549 cm^{-1} . This would help account for the difference in experimental and theoretical intensities as well as the fact that the predicted band at 1549 cm^{-1} is slightly red-shifted with respect to the experimental band at 1557 cm^{-1} .

A total of two additional conformers characterized by a $[\text{N}^-, \text{CO}, \text{CO}_{\text{sc}}]$ binding motif (shown in blue in Figure 4) were found, although they do not reproduce all of the experimental features well. Because the amino group, rather than carboxylic acid, is deprotonated in these complexes, there is no vibrational motion associated with the carboxylate CO stretch in the region around 1760 cm^{-1} . Predicted bands at 1546 (1551) and 1636 (1634) cm^{-1} may correspond to the 1557 and 1647 cm^{-1} bands in the $[\text{Zn}(\text{Gln}-\text{H})]^+$ spectrum. In the cases of the $[\text{N}^-, \text{CO}, \text{CO}_{\text{sc}}]$ spectra, the main bands in the $1300\text{--}1500\text{ cm}^{-1}$ region are attributed to COH bending (which cannot occur when deprotonation occurs at the carboxylic acid site), which results in the different band shape and frequencies.

Overall, the observed spectrum is consistent with the lowest-energy conformer $[\text{N},\text{CO}^-, \text{CO}_{\text{sc}}]-\text{gcgg}$, although the possibility that $[\text{N},\text{CO}^-, \text{CO}_{\text{sc}}]-\text{gggg}$ and $[\text{N}^-, \text{CO}, \text{CO}_{\text{sc}}]-\text{gtgt}$ conformers contribute cannot be excluded on the basis of the experimental data. However, the relatively high energies of these and all other conformers suggest that they are unlikely to be populated appreciably. An equilibrium distribution at 298 K would have a population of $\geq 99.95\%$ of the $[\text{N},\text{CO}^-, \text{CO}_{\text{sc}}]-\text{gcgg}$ conformer at all levels of theory.

Comparison of Experimental and Theoretical IR Spectra: $\text{CdCl}^+(\text{Gln})$. Similar to the results for $[\text{Zn}(\text{Gln}-\text{H})]^+$, the experimental IRMPD action spectrum of $\text{CdCl}^+(\text{Gln})$ is predicted fairly well by the tridentate $[\text{N},\text{CO}, \text{CO}_{\text{sc}}]$ conformers, Figure 5. Here, only subtle differences in the

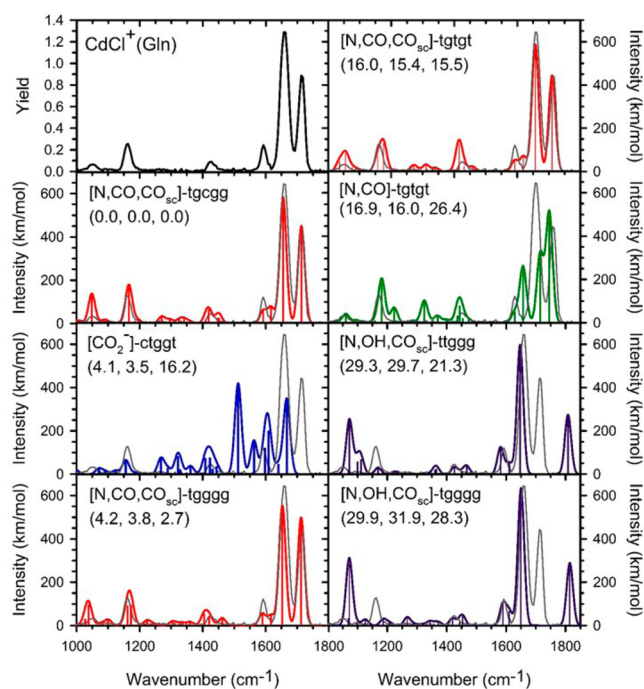


Figure 5. Comparison of the $\text{CdCl}^+(\text{Gln})$ experimental IRMPD action spectrum with IR spectra calculated at the B3LYP/def2-TZVP level of theory for low-lying conformers. Relative 0 K enthalpies (kJ/mol) are given at the B3LYP, B3P86, and MP2(full) levels, respectively.

spectra allow identification of the conformer that is likely formed experimentally. The main spectral features of the $\text{CdCl}^+(\text{Gln})$ spectrum are observed at 1048 , 1162 , 1427 , 1592 , 1662 , and 1717 cm^{-1} . There is very good agreement between the intense 1662 and 1717 cm^{-1} bands, which are probably the most diagnostic, and the corresponding bands in the $[\text{N},\text{CO}, \text{CO}_{\text{sc}}]$ spectra. The bands in the low-frequency region of the $\text{CdCl}^+(\text{Gln})$ spectrum are also in agreement with the predicted bands, with only minor blue shifts (of about 10 cm^{-1}) in the $[\text{N},\text{CO}, \text{CO}_{\text{sc}}]-\text{tgtgt}$ spectrum for the bands at 1048 and 1162 cm^{-1} and an equivalent red shift of the band in the $[\text{N},\text{CO}, \text{CO}_{\text{sc}}]-\text{tgggg}$ spectrum, corresponding to the 1048 cm^{-1} mode. Therefore, the most diagnostic band among the $\text{CdCl}^+(\text{Gln})$ and $[\text{N},\text{CO}, \text{CO}_{\text{sc}}]$ spectra for identification purposes is that at 1427 cm^{-1} . This band is best reproduced in the $[\text{N},\text{CO}, \text{CO}_{\text{sc}}]-\text{tgcg}$ spectrum, with the corresponding bands being red-shifted in the other two $[\text{N},\text{CO}, \text{CO}_{\text{sc}}]$ spectra. Thus, there is no indication that a combination of these $[\text{N},\text{CO}, \text{CO}_{\text{sc}}]$ conformers is needed to reproduce the experimental spectrum.

Additionally, for all $[\text{N},\text{CO}, \text{CO}_{\text{sc}}]$ conformers, there is a predicted band near 1620 cm^{-1} corresponding to the NH_2 bend of the backbone amino group that is absent in the experimental spectrum at that frequency. As mentioned above, this effect has been seen in similar systems, where it was concluded that strong anharmonic effects red-shift the NH_2 band in all cases. A red shift of the same magnitude shown in previous studies would produce a peak at $\sim 1595\text{ cm}^{-1}$ in the $[\text{N},\text{CO}, \text{CO}_{\text{sc}}]-\text{tgcg}$ spectrum, thus overlapping the predicted band at 1596 cm^{-1} . A combination of both bands in this frequency range would explain why the peak at 1592 cm^{-1} in the experimental spectrum exhibits a higher relative intensity as compared with the predicted spectra.

Figure 5 shows spectra for an additional four low-lying structures (4–32 kJ/mol higher in energy than the lowest-energy conformer), but the spectral features exhibited in those cases do not match the $\text{CdCl}^+(\text{Gln})$ spectrum to a degree that would suggest any of these conformers were formed experimentally. In particular, the zwitterionic $[\text{CO}_2^-]\text{-ctgg}$ conformer, calculated to lie only 4–17 kJ/mol higher than the lowest-energy conformer, has an intense band at 1513 cm^{-1} for which there is no evidence in the experimental spectrum. This band is primarily characterized by an NH_3 umbrella mode, a mode not present in the other conformers. Therefore, our spectral analysis confirms that the $[\text{N,CO,CO}_{\text{sc}}]\text{-tgccg}$ conformer is the complex formed experimentally, with no evidence for the zwitterionic complex. This agrees with the relative energies according to MP2(full) and B3LYP-GD3BJ but not B3LYP or B3P86. (An equilibrium distribution at 298 K of the three lowest-energy conformers according to B3LYP would have populations of 60, 20, and 20% for B3LYP; 51, 26, and 23% for B3P86; 63, 0.1, and 36% for MP2(full); and 74, 0.1, and 25% for B3LYP-GD3BJ.)

Overall Comparison. Here, we find it useful to give a more global analysis of the spectral features exhibited in the $[\text{Zn}(\text{Gln}-\text{H})]^+$ and $[\text{Cd}(\text{Gln})]^+$ IRMPD action spectra. As shown in Figures 4 and 5, the main spectral features in the $[\text{Zn}(\text{Gln}-\text{H})]^+$ complex are observed at 1053, 1167, 1218, 1557, 1647, and 1757 cm^{-1} , while those in the $\text{CdCl}^+(\text{Gln})$ spectrum appear at 1048, 1162, 1427, 1592, 1662, and 1717 cm^{-1} . The main bands that experience shifts are those corresponding to the CO stretching of the carboxylic acid carbonyl (1757 and 1717 cm^{-1}), amide CO stretching (1647 and 1662 cm^{-1}), and amide NH_2 scissoring (1557 and 1592 cm^{-1}). Note that the CO stretching of the carboxylic acid experiences the largest shift, with the Zn complex lying above that for Cd by 40 cm^{-1} , an effect that can be attributed primarily to deprotonation at the carboxylic site in $[\text{Zn}(\text{Gln}-\text{H})]^+$. The analogous effect was previously observed in a study of His complexes of Zn^{2+} and Cd^{2+} , where the shift is about 40 cm^{-1} .²¹ The other two modes show the opposite effect, where the Zn complex has a lower frequency than the Cd complex by 15 cm^{-1} for the amide CO stretch and 35 cm^{-1} for the amide NH_2 scissor motion. Such shifts have been previously observed in similar metal–amino acid systems and Asn complexes with Li^+ , Na^+ , K^+ , Rb^+ , Cs^+ , and Ba^{2+} .³⁵ This study concluded that more weakly bound metal cations perturb the vibrational motions less and, therefore, experience smaller shifts from the uncomplexed ligand. This can be directly related to the size of the metal center, as smaller metals allow shorter M–O and M–X distances, which translates into stronger electrostatic interactions between the metal and amino acid ligand.⁴⁹ This conclusion is also in agreement with the structural analysis in the previous section, which concludes that the Zn^{2+} metal center binds more tightly to the amino acid than Cd^{2+} . Other studies of zinc replacement, specifically with Cys and His, also conclude there is a higher degree of Zn^{2+} binding as compared with weaker binding affinity of Cd^{2+} centers.⁵⁰

The two bands in the $1050\text{--}1170\text{ cm}^{-1}$ region exhibit no significant shifting, as these stretches characterize motions of functional groups not involved in metal cation binding and, therefore, do not depend on the metal center. Additionally, there are unique features in each of the spectra. The $[\text{Zn}(\text{Gln}-\text{H})]^+$ complex exhibits a peak at 1218 cm^{-1} , corresponding primarily to CCH bending with a carboxylate CO stretch with additional contributions from NH_2 and CH_2 rocking. The

$\text{CdCl}^+(\text{Gln})$ spectrum shows a unique peak at 1427 cm^{-1} , which results largely from a CH_2 bend with additional contributions from amide CNH bending, CH_2 wagging, and minor COH bending. In both cases, the main vibrational motion is adjacent to the group most closely bound to the metal center, the carboxylate group in $[\text{Zn}(\text{Gln}-\text{H})]^+$ and the amide group in $\text{CdCl}^+(\text{Gln})$, which presumably allows the dipole changes that lead to the intensity differences. Overall, both the identity of the metal center and the mode of complexation have major effects on the main vibrational modes and the resulting IRMPD action spectra. In each of these cases, the shifts and relative intensities found experimentally are predicted well in the theoretical spectra.

Deamidation Pathways. Under biological conditions, the deamidation of Gln residues is known to proceed through a cyclic, glutarimide intermediate.⁹ Conformational and steric effects play obvious roles in controlling the rate of ring closure, which requires the transfer of a hydrogen to the amide NH_2 to form the NH_3 leaving group. This process can proceed straightforwardly within the $\text{CdCl}^+(\text{Gln})$ complex upon hydrogen transfer from the carboxylic acid group to the amide NH_2 , similar to the mechanism detailed for deamidation of both protonated and sodiated Asn.^{39,51} In contrast, because the $[\text{Zn}(\text{Gln}-\text{H})]^+$ complex has been deprotonated at the carboxylic acid, deamidation of this complex cannot occur readily and requires much more intramolecular rearrangement. Thus, the structural analysis of these complexes is an important factor in evaluating the deamidation properties of these and related systems.

As shown in Table 3, the M–O, M–N, and M–O_{sc} distances are considerably shorter in the $[\text{Zn}(\text{Gln}-\text{H})]^+$ complex as compared with those of the $\text{CdCl}^+(\text{Gln})$ complex, reflective of the smaller ionic radius of Zn^{2+} compared to Cd^{2+} and the anionic character of the deprotonated Gln ligand. These distances influence the relative binding strength exhibited by each complex and have a significant effect on the deamidation pathway observed in each case. Because the Zn^{2+} center is bound tightly in a tridentate orientation, the intramolecular rearrangement that is needed for hydrogen transfer to the amide nitrogen is hindered. Thus, the $[\text{Zn}(\text{Gln}-\text{H})]^+$ complex dissociates by the loss of Zn and CO_2 , which then allows the remaining organic ion to reorganize, such that deamidation occurs. For $\text{CdCl}^+(\text{Gln})$, where there is more conformational freedom because of the weaker interaction with the metal center and an available acidic hydrogen, deamidation is more facile. In addition to binding strength, conformational considerations affect the deamidation pathway. As shown by the $\angle\text{NMO}$, $\angle\text{NMO}_{\text{sc}}$, and $\angle\text{OMO}_{\text{sc}}$ values, the dihedral angles along the backbone of the $\text{CdCl}^+(\text{Gln})$ ground conformer are also less constrained. Again, this is representative of the larger ionic radius of Cd^{2+} , but these effects play an important role in the accessibility of the hydrogen that must be transferred for deamidation to proceed. Because the dihedral angles along the backbone of the $\text{CdCl}^+(\text{Gln})$ ground conformer adopt a conformation suitable for a cyclic structure to form more readily, the $\text{CdCl}^+(\text{Gln})$ system can undergo deamidation more directly than $[\text{Zn}(\text{Gln}-\text{H})]^+$. Overall, these trends suggest that the relative binding strength and conformation of the complexes are contributing factors regarding the favorable energetics of the dissociation of the Zn^{2+} center prior to deamidation, whereas the $\text{CdCl}^+(\text{Gln})$ easily deamidates with the metal center still intact.

In addition to structural considerations, insight into the deamidation pathway can be gathered from the IR spectra of the ions involved, specifically that of the $C_4H_9ON_2^+$ [101] product ion and its predicted spectrum. As noted above, formation of the deamidation product, reaction 2, is enhanced near the band at 1647 cm^{-1} in the experimental spectrum of $[Zn(\text{Gln}-\text{H})]^+$ compared with all other bands. As given in Figure S3, the calculated spectrum of $C_4H_9ON_2^+$ [101] shows several bands, but the most intense feature (by about an order of magnitude) is at 1647 cm^{-1} (amide and backbone amino NH_2 bending with small amide CO stretching contributions). This prediction is consistent with the observed frequency dependence for this sequential deamidation process. Thus, the activation of these modes at that frequency is clearly an important aspect of the deamidation process.

CONCLUSIONS

IRMPD action spectra for complexes of glutamine cationized with Zn^{2+} and Cd^{2+} were measured in the region of $1000\text{--}1800\text{ cm}^{-1}$ and were compared to those calculated at the B3LYP/6-311+G(d,p) and B3LYP/def2-TZVP levels of theory, respectively. For $[Zn(\text{Gln}-\text{H})]^+$ and $\text{CdCl}^+(\text{Gln})$, the theoretically determined ground conformer is found to reproduce the experimental spectra well. The $[\text{N},\text{CO}^-, \text{CO}_{\text{sc}}]\text{-gcgg}$ conformer of the $[Zn(\text{Gln}-\text{H})]^+$ complex is confirmed to be the complex present experimentally, although small contributions from higher-lying $[\text{N},\text{CO}^-, \text{CO}_{\text{sc}}]$ conformers could be present. For the $\text{CdCl}^+(\text{Gln})$ complex, the experimental IRMPD spectrum was predicted fairly well by three low-lying tridentate $[\text{N},\text{CO}, \text{CO}_{\text{sc}}]$ conformers, with the $[\text{N},\text{CO}, \text{CO}_{\text{sc}}]\text{-tgccg}$ lowest-energy conformer providing the best match with the experimental spectrum.

Our discussion of changes in vibrational modes and geometric parameters also gives insight into the binding strength of the metal center within the complex, a characterization instrumental in determining the metal dependence of these and other biological systems. The shorter M–O and M–X distances of the $[Zn(\text{Gln}-\text{H})]^+$ complex should lead to stronger metal–amino acid binding compared to binding observed in the $\text{CdCl}^+(\text{Gln})$ complex. Dihedral angles in the $\text{CdCl}^+(\text{Gln})$ complex are also significantly less constrained, allowing the more facile formation of a cyclic structure that is necessary for deamidation to occur. We directly correlated these findings to the observation of differing pathways for deamidation, as the Zn^{2+} center dissociates prior to deamidation, whereas deamidation progresses in the $\text{CdCl}^+(\text{Gln})$ complex with the Cd^{2+} center still bound to the Gln ligand. The characteristic vibrational modes in the measured spectra also provide valuable information with respect to the metal dependence of the system (as given by the band shifts observed in our spectral results), although some shifts arise from the inherent difference in binding between Zn^{2+} and anionic (Gln–H) versus CdCl^+ and neutral Gln. Overall, the results presented here provide valuable fundamental information for the continuation of our metal–amino acid studies, specifically regarding the metal dependence of biologically important systems.

ASSOCIATED CONTENT

Supporting Information

The Supporting Information is available free of charge on the ACS Publications website at DOI: 10.1021/acs.jpcc.5b06528.

Additional information includes figures showing spectral comparisons between experimental IRMPD and calculated spectra and the calculated spectrum for the $C_4H_9ON_2^+$ [101] product and tables showing the vibrational frequencies and IR intensities of low-energy conformers, as well as the relative enthalpies and free energies of additional higher-energy complexes. (PDF)

AUTHOR INFORMATION

Corresponding Author

*E-mail: armentrout@chem.utah.edu.

Notes

The authors declare no competing financial interest.

ACKNOWLEDGMENTS

Financial support for this work was provided by the National Science Foundation, grants CHE-1359769 and PIRE-0730072. The skillful assistance of the FELIX staff is gratefully acknowledged. In addition, a grant of computer time from the Center for High Performance Computing at the University of Utah is greatly appreciated.

REFERENCES

- (1) Robinson, N. E.; Robinson, A. B. *Molecular Clocks: Deamidation of Asparaginyl and Glutaminyl Residues in Peptides and Proteins*. Althouse Press: Cave Junction, OR, 2004.
- (2) Lindner, H.; Helliger, W. Age-Dependent Deamidation of Asparagine Residues in Proteins. *Exp. Gerontol.* **2001**, *36*, 1551–1563.
- (3) Robinson, N. E.; Robinson, A. B. Deamidation of Human Proteins. *Proc. Natl. Acad. Sci. U. S. A.* **2001**, *98*, 12409–12413.
- (4) Heaton, A. L.; Ye, S. J.; Armentrout, P. B. Experimental and Theoretical Studies of Sodium Cation Complexes of the Deamidation and Dehydration Products of Asparagine, Glutamine, Aspartic Acid, and Glutamic Acid. *J. Phys. Chem. A* **2008**, *112*, 3328–3338.
- (5) Heaton, A. L.; Armentrout, P. B. Experimental and Theoretical Studies of Potassium Cation Interactions with the Acidic Amino Acids and Their Amide Derivatives. *J. Phys. Chem. B* **2008**, *112*, 12056–12065.
- (6) Wilson, J.; van Doorn, N. L.; Collins, M. J. Assessing the Extent of Bone Degradation Using Glutamine Deamidation in Collagen. *Anal. Chem.* **2012**, *84*, 9041–9048.
- (7) Robinson, N. E.; Robinson, A. B. Prediction of Primary Structure Deamidation Rates of Asparaginyl and Glutaminyl Peptides through Steric and Catalytic Effects. *J. Pept. Res.* **2004**, *63*, 437–448.
- (8) Robinson, N. E.; Robinson, A. B. Molecular Clocks. *Proc. Natl. Acad. Sci. U. S. A.* **2001**, *98*, 944–949.
- (9) Li, X.; Lin, C.; O'Connor, P. B. Glutamine Deamidation: Differentiation of Glutamic Acid and γ -Glutamic Acid in Peptides by Electron Capture Dissociation. *Anal. Chem.* **2010**, *82*, 3606–3615.
- (10) Catterall, J. B.; Hsueh, M. F.; Stabler, T. V.; McCudden, C. R.; Bolognesi, M.; Zura, R.; Jordan, J. M.; Renner, J. B.; Feng, S.; Kraus, V. B. Protein Modification by Deamidation Indicates Variations in Joint Extracellular Matrix Turnover. *J. Biol. Chem.* **2012**, *287*, 4640–4651.
- (11) Monoi, H.; Futaki, S.; Kugimiya, S.; Minakata, H.; Yoshihara, K. Poly-L-Glutamine Forms Cation Channels: Relevance to the Pathogenesis of the Polyglutamine Diseases. *Biophys. J.* **2000**, *78*, 2892–2899.
- (12) Hensley, C. T.; Wasti, A. T.; DeBerardinis, R. J. Glutamine and Cancer: Cell Biology, Physiology, and Clinical Opportunities. *J. Clin. Invest.* **2013**, *123*, 3678–3684.
- (13) Rajagopalan, K. N.; DeBerardinis, R. J. Role of Glutamine in Cancer-Therapeutic and Imaging Implications. *J. Nucl. Med.* **2011**, *52*, 1005–1008.
- (14) Iuchi, S.; Kuldell, N. *Zinc Finger Proteins from Atomic Contact to Cellular Function*. Kluwer Academic/Plenum: New York, 2005.

- (15) Iuchi, S. Three Classes of C₂H₂ Zinc Finger Proteins. *Cell. Mol. Life Sci.* **2001**, *58*, 625–635.
- (16) Laity, J. H.; Lee, B. M.; Wright, P. E. Zinc Finger Proteins: New Insights into Structural and Functional Diversity. *Curr. Opin. Struct. Biol.* **2001**, *11*, 39–46.
- (17) Wolfe, S. A.; Nekludova, L.; Pabo, C. O. DNA Recognition by Cys₂His₂ Zinc Finger Proteins. *Annu. Rev. Biophys. Biomol. Struct.* **2000**, *39*, 183–212.
- (18) Malgieri, G.; Palmieri, M.; Esposito, S.; Maione, V.; Russo, L.; Baglivo, I.; de Paola, I.; Milardi, D.; Diana, D.; Zaccaro, L.; et al. Zinc to Cadmium Replacement in the Prokaryotic Zinc-Finger Domain. *Metallomics* **2014**, *6*, 96–104.
- (19) Malgieri, G.; Zaccaro, L.; Leone, M.; Bucci, E.; Esposito, S.; Baglivo, I.; del Gatto, A.; Russo, L.; Scandurra, R.; Pedone, P. V.; et al. Zinc to Cadmium Replacement in the A. Thaliana Superman Cys₂His₂ Zinc Finger Induces Structural Rearrangements of Typical DNA Base Determinant Positions. *Biopolymers* **2011**, *95*, 801–810.
- (20) Citir, M.; Hinton, C. S.; Oomens, J.; Steill, J. D.; Armentrout, P. B. Infrared Multiple Photon Dissociation Spectroscopy of Cationized Histidine: Effects of Metal Cation Size on Gas-Phase Conformation. *J. Phys. Chem. A* **2012**, *116*, 1532–1541.
- (21) Hofstetter, T. E.; Howder, C.; Berden, G.; Oomens, J.; Armentrout, P. B. Structural Elucidation of Biological and Toxicological Complexes: Investigation of Monomeric and Dimeric Complexes of Histidine with Multiply Charged Transition Metal (Zn and Cd) Cations Using IR Action Spectroscopy. *J. Phys. Chem. B* **2011**, *115*, 12648–12661.
- (22) Citir, M.; Stennett, E. M. S.; Oomens, J.; Steill, J. D.; Rodgers, M. T.; Armentrout, P. B. Infrared Multiple Photon Dissociation Spectroscopy of Cationized Cysteine: Effects of Metal Cation Size on Gas-Phase Conformation. *Int. J. Mass Spectrom.* **2010**, *297*, 9–17.
- (23) Coates, R. A.; McNary, C. P.; Boles, G. C.; Berden, G.; Oomens, J.; Armentrout, P. B. Structural Characterization of Gas-Phase Cysteine and Cysteine Methyl Ester Complexes with Zinc and Cadmium Dications by Infrared Multiple Photon Dissociation Spectroscopy. *Phys. Chem. Chem. Phys.* **2015**, in press. DOI: 10.1039/C5CP01500F.
- (24) Oepts, D.; van der Meer, A. F. G.; van Amersfoort, P. W. The Free-Electron-Laser User Facility Felix. *Infrared Phys. Technol.* **1995**, *36*, 297–308.
- (25) Valle, J. J.; Eyler, J. R.; Oomens, J.; Moore, D. T.; van der Meer, A. F. G.; von Helden, G.; Meijer, G.; Hendrickson, C. L.; Marshall, A. G.; Blakney, G. T. Free Electron Laser-Fourier Transform Ion Cyclotron Resonance Mass Spectrometry Facility for Obtaining Infrared Multiphoton Dissociation Spectra of Gaseous Ions. *Rev. Sci. Instrum.* **2005**, *76*, 023103.
- (26) Polfer, N. C.; Oomens, J.; Moore, D. T.; von Helden, G.; Meijer, G.; Dunbar, R. C. Infrared Spectroscopy of Phenylalanine Ag(I) and Zn(II) Complexes in the Gas Phase. *J. Am. Chem. Soc.* **2006**, *128*, 517–525.
- (27) Polfer, N. C.; Oomens, J. Reaction Products in Mass Spectrometry Elucidated with Infrared Spectroscopy. *Phys. Chem. Chem. Phys.* **2007**, *9*, 3804–3817.
- (28) Oomens, J.; Sartakov, B. G.; Meijer, G.; von Helden, G. Gas-Phase Infrared Multiple Photon Dissociation Spectroscopy of Mass-Selected Molecular Ions. *Int. J. Mass Spectrom.* **2006**, *254*, 1–19.
- (29) Polfer, N. C. Infrared Multiple Photon Dissociation Spectroscopy of Trapped Ions. *Chem. Soc. Rev.* **2011**, *40*, 2211–2221.
- (30) Dunbar, R. C. Infrared Radiative Cooling of Isolated Polyatomic Molecules. *J. Chem. Phys.* **1989**, *90*, 7369–7375.
- (31) Frisch, M. J.; Trucks, G. W.; Schlegel, H. B.; Scuseria, G. E.; Robb, M. A.; Cheeseman, J. R.; Scalmani, G.; Barone, V.; Mennucci, B.; Petersson, G. A.; et al. Gaussian 09, Revision D.01; Gaussian, Inc.: Wallingford, CT, 2009.
- (32) Weigend, F.; Ahlrichs, R. Def2-Svp Basis Sets. *Phys. Chem. Chem. Phys.* **2005**, *7*, 3297–3305.
- (33) Andrae, D.; Haeussermann, U.; Dolg, M.; Stoll, H.; Preuss, H. Energy-Adjusted Ab Initio Pseudopotentials for the Second and Third Row Transition Elements. *Theor. Chim. Acta* **1990**, *77*, 123–141.
- (34) Feller, D. The Role of Databases in Support of Computational Chemistry Calculations. *J. Comput. Chem.* **1996**, *17*, 1571–1586.
- (35) Heaton, A. L.; Bowman, V. N.; Oomens, J.; Steill, J. D.; Armentrout, P. B. Infrared Multiple Photon Dissociation Spectroscopy of Cationized Asparagine: Effects of Alkali-Metal Cation Size on Gas-Phase Conformation. *J. Phys. Chem. A* **2009**, *113*, 5519–5530.
- (36) Grimme, S.; Ehrlich, S.; Goerigk, L. Effect of the Damping Function in Dispersion Corrected Density Functional Theory. *J. Comput. Chem.* **2011**, *32*, 1456–1465.
- (37) Lemaire, J.; Boissel, P.; Heninger, M.; Mauclaire, G.; Bellec, G.; Mestdagh, H.; Simon, A.; Le Caer, S.; Ortega, J. M.; Glotin, F.; et al. Gas Phase Infrared Spectroscopy of Selectively Prepared Ions. *Phys. Rev. Lett.* **2002**, *89*, 273002.
- (38) Berglund, M.; Wieser, M. E. Isotopic Compositions of the Elements 2009. *Pure Appl. Chem.* **2011**, *83*, 397–410.
- (39) Heaton, A. L.; Armentrout, P. B. Thermodynamics and Mechanism of Protonated Asparagine Decomposition. *J. Am. Soc. Mass Spectrom.* **2009**, *20*, 852–866.
- (40) Allinger, N. L.; Profeta, S. J. The Torsional Potential Function for N-Butane. *J. Comput. Chem.* **1980**, *1*, 181–184.
- (41) Fadda, E.; Woods, R. J. Contribution of the Empirical Dispersion Correction on the Conformation of Short Alanine Peptides Obtained by Gas-Phase QM Calculations. *Can. J. Chem.* **2013**, *91*, 859–865.
- (42) Bush, M. F.; Oomens, J.; Saykally, R. J.; Williams, E. R. Alkali Metal Ion Binding to Glutamine and Glutamine Derivatives Investigated by Infrared Action Spectroscopy and Theory. *J. Phys. Chem. A* **2008**, *112*, 8578–8584.
- (43) Shannon, R. D. Revised Effective Ionic Radii and Systematic Studies of Interatomic Distances in Halides and Chalcogenides. *Acta Crystallogr., Sect. A: Cryst. Phys., Diffr., Theor. Gen. Crystallogr.* **1976**, *A32*, 751–767.
- (44) Carl, D. R.; Cooper, T. E.; Oomens, J.; Steill, J. D.; Armentrout, P. B. Infrared Multiple Photon Dissociation Spectroscopy of Cationized Methionine: Effects of Alkali-Metal Cation Size on Gas-Phase Conformation. *Phys. Chem. Chem. Phys.* **2010**, *12*, 3384–3398.
- (45) Armentrout, P. B.; Rodgers, M. T.; Oomens, J.; Steill, J. D. Infrared Multiphoton Dissociation Spectroscopy of Cationized Serine: Effects of Alkali-Metal Cation Size on Gas-Phase Conformation. *J. Phys. Chem. A* **2008**, *112*, 2248–2257.
- (46) Rodgers, M. T.; Armentrout, P. B.; Oomens, J.; Steill, J. D. Infrared Multiphoton Dissociation Spectroscopy of Cationized Threonine: Effects of Alkali-Metal Cation Size on Gas-Phase Conformation. *J. Phys. Chem. A* **2008**, *112*, 2258–2267.
- (47) Oomens, J.; Moore, D. T.; Meijer, G.; von Helden, G. Infrared Multiple Photon Dynamics and Spectroscopy of Cationic PABA and Its Dehydroxylated Fragment Ion. *Phys. Chem. Chem. Phys.* **2004**, *6*, 710–718.
- (48) Sinclair, W. E.; Pratt, D. W. Structure and Vibrational Dynamics of Aniline and Aniline-Ar from High Resolution Electronic Spectroscopy in the Gas Phase. *J. Chem. Phys.* **1996**, *105*, 7942–7956.
- (49) Austin, C. A.; Rodgers, M. T. Alkali Metal Cation-Hexacyclen Complexes: Effects of Alkali Metal Cation Size on the Structure and Binding Energy. *J. Phys. Chem. A* **2014**, *118*, 5488–5500.
- (50) Zhou, Y.; Zhang, N.; Li, L.; Ru, B. The Cysteine-to-Histidine Substitution in B Domain of Metallothionein Enhances Its Zinc Binding Ability. *Biochim. Biophys. Acta, Gen. Subj.* **2000**, *7*, 9–16.
- (51) Heaton, A. L.; Moision, R. M.; Armentrout, P. B. Experimental and Theoretical Studies of Sodium Cation Interactions with the Acidic Amino Acids and Their Amide Derivatives. *J. Phys. Chem. A* **2008**, *112*, 3319–3327.